Chinese Chemical Letters 34 (2023) 107611

Contents lists available at ScienceDirect

Chinese Chemical Letters

journal homepage: www.elsevier.com/locate/cclet

# From design to biological mechanism evaluation of phenylalanine-bearing HIV-1 capsid inhibitors targeting a vital assembly interface

Shujing Xu[a], Lin Sun[a], Waleed A. Zalloum[b], Xujie Zhang[a], Tianguang Huang[a], Dang Ding[a], Yucen Tao[a], Fabao Zhao[a], Shenghua Gao[a], Dongwei Kang[a], Erik De Clercq[c], Christophe Pannecouque[c,*], Alexej Dick[d,*], Simon Cocklin[d,*], Xinyong Liu[a,*], Peng Zhan[a,*]

[a] Department of Medicinal Chemistry, Key Laboratory of Chemical Biology (Ministry of Education), School of Pharmaceutical Sciences, Shandong University, Ji'nan 250012, China
[b] Department of Pharmacy, Faculty of Health Science, American University of Madaba, Amman 11821, Jordan
[c] Rega Institute for Medical Research, Laboratory of Virology and Chemotherapy, K.U. Leuven, Leuven B 3000, Belgium
[d] Department of Biochemistry & Molecular Biology, Drexel University College of Medicine, Philadelphia, PA 19102, United States

ARTICLE INFO

*Article history:*
Received 21 March 2022
Revised 12 June 2022
Accepted 14 June 2022
Available online 18 June 2022

*Keywords:*
HIV-1
Capsid inhibitor
Assembly
NTD-CTD interface
Drug design

ABSTRACT

HIV-1 capsid protein (CA) has emerged as a promising target for antiviral treatment considering its structural and regulatory roles in HIV-1 replication. Here, we disclose the design, synthesis, biological assessment, and mechanism investigation of a novel series of phenylalanine derivatives gained by further structural modification of **PF74**. The newly synthesized compounds demonstrated potent anti-HIV activity, represented by **7n** displayed anti-HIV-1 activity 6.25-fold better than **PF74**, and **7h** showed anti-HIV-2 activity with nearly 139 times improved efficacy over **PF74**. Surface plasmon resonance (SPR) studies of representative compounds proved that HIV-1 CA was the binding target. Competitive SPR studies using CPSF6 and NUP153 peptides identified that **7n** binds to a vital CA assembly interface between the N-terminal and C-terminal domain (NTD-CTD interface). Action stage determination assay revealed that the newly synthesized compounds were antiviral with a dual-stage inhibitory profile. Molecular dynamics (MD) simulations offered the crucial foundation for the hopeful antiviral potency of **7n**. Besides, **7m** and **7n** modestly increased metabolic stabilities in human liver microsome (HLM) and human plasma compared to **PF74**. Overall, these studies offer valuable insights and can regard as the beginning for succedent medicinal chemistry endeavors to discover promising HIV capsid inhibitors with improved efficacy and better drug-like characteristics.



Acquired immunodeficiency syndrome (AIDS) is a chronic infectious disease infected by human immunodeficiency virus (HIV) [1]. HIV is an RNA retrovirus divided into HIV-1 and HIV-2 subtypes [2], of which HIV-1 is the main epidemic pathogen; as of 2020, it is estimated that 37.7 million individuals live with HIV-1 [3]. HIV-2 is prevalent in West Africa, and it has spread to neighboring countries with socioeconomic links to the region [4]. Combinatorial antiretroviral therapy (cART) is an anti-HIV drug combination targeted at several stages of the virus life cycle and has shown to be effective in preventing HIV infection [5,6]. Nevertheless, the long-term use of cART has been hampered by the establishment of substantially cross-resistant HIV-1 strains and cumulative medication toxicities [7–9]. Additionally, it has been reported that drug resistance of HIV-2 may occur earlier than HIV-1 and selectively mutate at different sites [10]. Therefore, it is an urgent need for researchers to develop new classes of anti-AIDS agents with unique action modalities or targets, and reduced side effects.

HIV-1 capsid protein (CA), a widely conserved protein required for HIV-1 replication, participating in multiple steps of the viral life cycle, has risen to prominence as an attractive target for therapeutic intervention [11–13]. Mature CA consists of about 1500 monomers, mainly arranged into hexameric lattices but also into 12 pentamers that induce curvatures at the core-periphery to assemble a closed conical ship [14,15]. CA monomer is made up of two alpha-helical domains, the N-terminal domain (NTD) and

* Corresponding authors:
*E-mail addresses:* christophe.pannecouque@kuleuven.be (C. Pannecouque), ad3474@drexel.edu (A. Dick), sc349@drexel.edu (S. Cocklin), xinyongl@sdu.edu.cn (X. Liu), zhanpeng1982@sdu.edu.cn (P. Zhan).

https://doi.org/10.1016/j.cclet.2022.06.034
1001-8417/

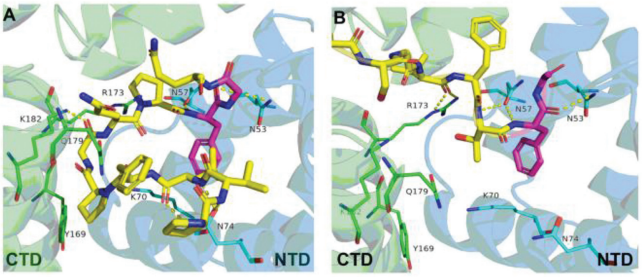


**Fig. 1.** Crystal structure of HIV-1 CA in complex with (A) CPSF6 peptide (PDB code: 4WYM) and (B) NUP153 peptide (PDB code: 6AYA). The figures are generated in PyMOL (www.pymol.org).

C-terminal domain (CTD), connecting by a short flexible linker [16]. A conserved interprotomer pocket (namely NTD-CTD interface) exists in the structure of assembled CA multimers, which has been proved to interact with host-cell proteins such as cleavage and polyadenylation specificity factor-6 (CPSF6) and nucleoporin 153 (NUP153) (Fig. 1) [17]. The CA-CPSF6 interaction promotes the pre-integration complexes (PICs) to enter the nucleus, modulates nuclear localization, and integrates viral reverse transcripted DNA into the transcriptional active areas of host genes [18,19]. NUP153, as a nucleoporin, is also critical for the nuclear transport of viral PICs [20,21]. Disruption of these interactions through mutagenesis can interfere with HIV-1 replication, suggesting that NTD-CTD interface is a major target for inhibitor design.

Consistent with this speculation, the NTD-CTD interface has been defined as the mature binding site of the CA-targeted small molecule inhibitor **PF-3450074** (**PF74**, Fig. 2) [22,23]. In agreement with the binding multifunction of this pocket, **PF74** exhibits a concentration-dependent bimodal mechanism for its antiviral activity: At lower concentrations, it competes with host factors CPSF6 and NUP153 to influence nuclear entry; and at higher concentrations, it interrupts uncoating and reverse transcription, probably by altering inter-hexamer interactions [24,25]. However, **PF74** was unable to reach clinical development owing to its insufficient antiviral efficacy and metabolic instability. Additionally, the binding site of **PF74** only partially overlaps with CPSF6 and NUP153, which provides sufficient space within the NTD-CTD interface for further modification of **PF74**.

An examination of the **PF74**-CA complex structure indicates that there are multiple polar amino acid residues (such as Tyr169, Arg173, Lys182) in the NTD-CTD interface which does not form significant interactions with **PF74**, indicating a new site for structural optimization to improve antiviral activity, anti-drug resistance, and druggability. In this paper, to further enhance the potency and drug-like features, we selected **PF74** as the lead compound, designed and synthesized a series of new small molecule moderators of capsid assembly to target the hot spot residues in NTD-CTD interface based on a structure-guided design strategy and drug-like parameters (such as $Fsp^3$)-inspired optimization (Fig. 2) [26]. It has been proven that introducing a methoxy at the *para*-position of the aniline and replacing phenylalanine with 3,5-difluorophenylalanine is favorable for antiviral activity; hence, we kept the methoxy–bearing aniline substituent and 3,5-difluorophenylalanine on basic skeleton of **PF74**. Further, employing piperazinone rich in $sp^3$ hybrid carbon as a linker, we replaced the indole moiety with different substituted benzenesulfonyl groups bearing multiple hydrogen bond donors or receptors, aiming to form additional interactions with surrounding key residues in the NTD-CTD interface to improve binding affinity and drug-like qualities. Herein, the newly synthesized compounds were screened for antiviral activity and conducted to structure-activity relationship (SAR) analysis. Furthermore, we used surface plasmon resonance (SPR), action stage determination studies, and molecular dynamics (MD) simulations to investigate the mechanism of action (MOA) of these compounds. Finally, the stability experiments of representative compounds **7b**, **7m**, **7n** were also carried out in human liver microsome (HLM) and human plasma, respectively.

The target compounds **7a**-**7n** were prepared according to the general Scheme 1. Briefly, (*tert*–butoxycarbonyl)-3,5-difluoro-L-phenylalanine (**1**) was treated with 4–methoxy-*N*-methylaniline and 2-(7-aza-1*H*-benzotriazole-1-yl)-1,1,3,3-tetramethyluronium hexafluoro (HATU) in the presence of *N*,*N*-diisopropylethyl-amine (DIEA) and dichloromethane (DCM) to give **2**, followed by the removal of *tert*–butyloxycarbonyl (Boc) protection using trifluoroacetic acid (TFA) to yield the free amine **3**. The acylation of **3** with bromoacetic acid in DCM resulted in the crucial intermediate **4**. Further, **4** was reacted with 1-Boc-3-oxopiperazine *via* a nucleophilic substitution ($SN_2$) reaction to afford intermediate **5**. Removing the Boc protection of **5** yielded the free amine **6**, which was acylated with the matching substituted benzenesulfonyl

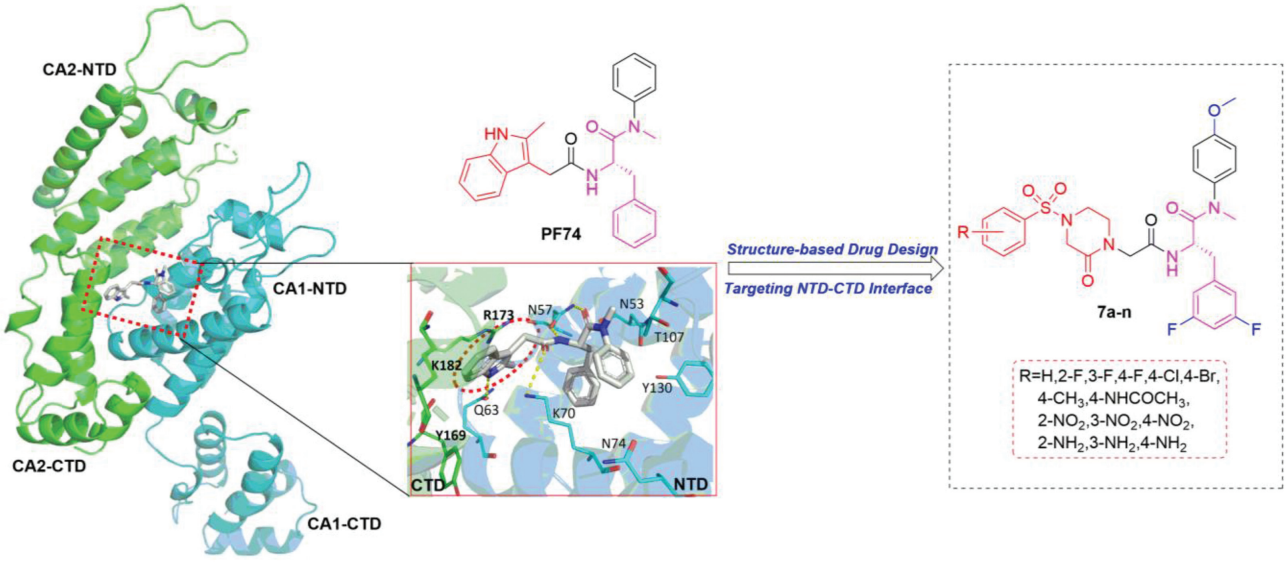


**Fig. 2.** Design principle of novel small molecule inhibitors targeting HIV-1 CA NTD-CTD interface. The figures are generated in PyMOL (www.pymol.org).

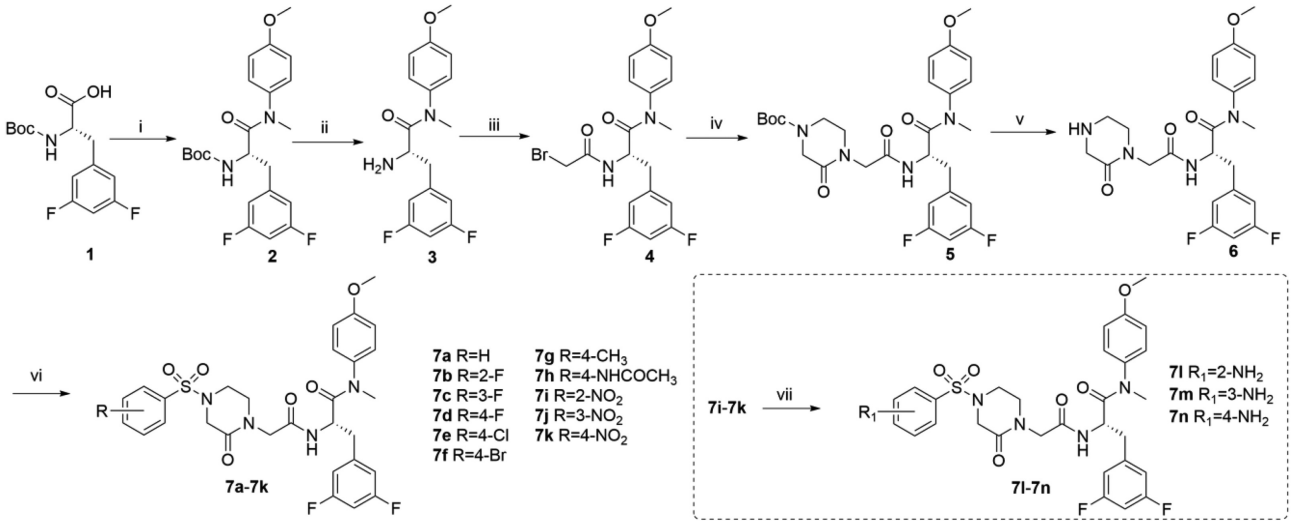


**Scheme 1.** Reagents and conditions: (i) 4-Methoxy-*N*-methylaniline, HATU, DIEA, 0 °C to r.t.; (ii) TFA, DCM, r.t.; (iii) Bromoacetic acid, HATU, DIEA, 0 °C to r.t.; (iv) 1-Boc-3-oxopiperazine, $Cs_2CO_3$, DMF, 45 °C; (v) TFA, DCM, r.t.; (vi) TEA, DCM, r.t.; (vii) $H_2$, 10%Pd·C, DCM, r.t.

**Table 1**
Anti-HIV activity and cytotoxicity in MT-4 Cells infected with HIV-1 $III_B$ virus and HIV-2 ROD virus.

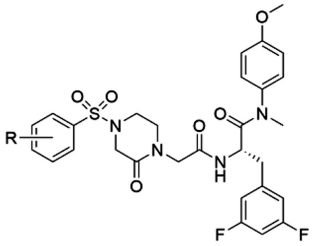

| Compd. | R | $EC_{50}$[a] (μmol/L) | | | $CC_{50}$[c] (μmol/L) | SI[d] | |
|---|---|---|---|---|---|---|---|
| | | $III_B$ | ROD | Ratio[b] | | $III_B$ | ROD |
| **7a** | H | 0.20 ± 0.05 | 0.10 ± 0.03 | 2.00 | 113.90 ± 6.55 | 569.50 | 1139.00 |
| **7b** | 2-F | 0.18 ± 0.05 | 0.09 ± 0.03 | 2.00 | 180.69 ± 11.36 | 1003.83 | 2007.67 |
| **7c** | 3-F | 0.24 ± 0.10 | 0.12 ± 0.04 | 2.00 | >202.21 | >842.54 | >1685.08 |
| **7d** | 4-F | 0.79 ± 0.15 | 0.36 ± 0.32 | 2.19 | 19.19 ± 2.73 | 24.29 | 53.31 |
| **7e** | 4-Cl | 0.93 ± 0.20 | 0.44 ± 0.16 | 2.11 | 9.05 ± 0.74 | 9.73 | 20.57 |
| **7f** | 4-Br | 0.86 ± 0.24 | 0.35 ± 0.18 | 2.46 | 13.24 ± 2.77 | 15.40 | 37.83 |
| **7g** | 4-$CH_3$ | 0.91 ± 0.36 | 0.12 ± 0.03 | 7.58 | >203.52 | >223.65 | >1696.00 |
| **7h** | 4-$NHCOCH_3$ | 0.21 ± 0.06 | 0.03 ± 0.01 | 7.00 | 91.58 ± 8.70 | 436.10 | 3052.67 |
| **7i** | 2-$NO_2$ | 2.84 ± 0.29 | 1.19 ± 0.36 | 2.39 | 94.87 ± 21.85 | 33.40 | 79.72 |
| **7j** | 3-$NO_2$ | 1.49 ± 0.64 | 0.17 ± 0.03 | 8.76 | 83.87 ± 28.33 | 56.29 | 493.35 |
| **7k** | 4-$NO_2$ | 1.01 ± 0.20 | 0.48 ± 0.36 | 2.10 | 14.85 ± 3.87 | 14.70 | 30.94 |
| **7l** | 2-$NH_2$ | 0.52 ± 0.11 | 0.14 ± 0.03 | 3.71 | 63.62 ± 26.54 | 122.35 | 454.43 |
| **7m** | 3-$NH_2$ | 0.16 ± 0.05 | 0.11 ± 0.02 | 1.45 | 108.60 ± 2.00 | 678.75 | 987.27 |
| **7n** | 4-$NH_2$ | 0.12 ± 0.01 | 0.05 ± 0.01 | 2.40 | 117.23 ± 5.62 | 976.92 | 2344.60 |
| **PF74** | | 0.75 ± 0.33 | 4.16 ± 2.02 | 0.18 | 32.27 ± 2.94 | 43.03 | 7.76 |

[a] $EC_{50}$: concentration of compound required to achieve 50% protection of MT-4 cell cultures against HIV-1-induced cytotoxicity, as determined by the MTT method.
[b] $EC_{50(IIIB)}/EC_{50(ROD)}$ ratio.
[c] $CC_{50}$: concentration required to reduce the viability of mock-infected cell cultures by 50%, as determined by the MTT method.
[d] SI: selectivity index, the ratio of $CC_{50}/EC_{50}$.

chloride to generate the desired compounds **7a**-**7k**. The amino analogues **7l**-**7n** were created by hydrogenating the nitro group of **7i**-**7k**.

Compounds in this program were evaluated for their antiviral activity in MT-4 cells based MTT assay containing wild-type (WT) HIV-1 $III_B$ and HIV-2 (ROD). The selectivity index (SI value, $CC_{50}/EC_{50}$) of the test compounds was determined by assessing compound toxicity against MT-4 cells in parallel using an MTT assay. Table 1 displayed the findings of the analysis.

The majority of the compounds in this series demonstrated remarkable anti-HIV-1 activities in submicromolar levels, of which seven compounds exceeded **PF74** ($EC_{50}$ = 0.75 μmol/L). The unsubstituted benzene (**7a**, $EC_{50}$ = 0.20 μmol/L) and fluorine substitution at the meta- or ortho-position [**7b** ($EC_{50}$ = 0.18 μmol/L), **7c** ($EC_{50}$ = 0.24 μmol/L)] led to a significant improvement in efficacy and SI values. However, the efficacy of these compounds with a halogen modification at the para-position on the benzene [**7d** ($EC_{50}$ = 0.79 μmol/L), **7e** ($EC_{50}$ = 0.93 μmol/L), **7f** ($EC_{50}$ = 0.86 μmol/L)] was modest decreased; these compounds also exhibited low SI values illustrating that the decrease in efficacy might be ascribed to a concurrent increase in toxicity. The methyl substitution at the para-position (**7g**, $EC_{50}$ = 0.91 μmol/L) also resulted in a modestly decrease in potency but with a marked increased SI value indicating a

decrease in toxicity. An acetamido group at the para-position contributed to a 3.57-fold increase in potency and >10 SI value (**7h**, $EC_{50}$ = 0.21 μmol/L). Compounds **7i** ($EC_{50}$ = 2.84 μmol/L), **7j** ($EC_50$ = 1.49 μmol/L), **7k** ($EC_{50}$ = 1.01 μmol/L) containing a nitro substitution had decreased anti-HIV-1 activity along with equaled or lower SI values. Notably, the amino substitution at the *ortho*-, *meta*- or *para*-position [**7l** ($EC_{50}$ = 0.52 μmol/L), **7m** ($EC_{50}$ = 0.16 μmol/L), **7n** ($EC_{50}$ = 0.12 μmol/L)] led to a rise in potency while maintaining low toxicity, resulting in an increase in the SI value. Interestingly, among the nitro/amino substitution, a clear SAR was observed that the hydrogen-bond donor (amino) has the same activity order as the hydrogen-bond receptor (nitro): *para*-position > *meta*-position > *ortho*-position. Finally, the identification of **7n** represented a 6.25-fold improvement in potency over the lead compound **PF74**.

Exceptionally, all of the compounds demonstrated improved anti-HIV-2 potency and higher SI values than **PF74** ($EC_{50}$ = 4.16 μmol/L, SI = 43.03). Among them, **7h** was shown to be the most potent of the series against HIV-2, with an $EC_{50}$ value of 0.03 μmol/L, which was 139-fold than **PF74**. Take the unsubstituted benzene compound **7a** ($EC_{50}$ = 0.10 μmol/L) as a reference: (i) Among the *ortho*-substituted benzene derivatives, substitution with 2-fluorine (**7b**, $EC_{50}$ = 0.09 μmol/L) and 2-amino (**7l**, $EC_{50}$ = 0.14 μmol/L) equaled to **7a**. However, the introduction of 2-nitro (**7i**, $EC_{50}$ = 1.19 μmol/L) decreased the antiviral activity. (ii) Among the meta-substituted benzene derivatives, substitution with 3-fluorine (**7c**, $EC_{50}$ = 0.12 μmol/L) and 3-amino (**7m**, $EC_{50}$ = 0.11 μmol/L) led to equaled efficacy compared with **7a**, and 3-nitro (**7j**, $EC_{50}$ = 0.17 μmol/L) showed a modest decrease in potency; (iii) Among the *para*-substituted benzene derivatives, the electron-donating groups [4-methyl (**7g**, $EC_{50}$ = 0.12 μmol/L), 4-acetamido (**7h**, $EC_{50}$ = 0.03 μmol/L), 4-amino (**7n**, $EC_{50}$ = 0.05 μmol/L)] were advantageous for activity, while the electron-withdrawing groups such as 4-fluorine (**7d**, $EC_{50}$ = 0.36 μmol/L), 4-chlorine (**7e**, $EC_{50}$ = 0.44 μmol/L), 4-bromine (**7f**, $EC_{50}$ = 0.35 μmol/L) and 4-nitro (**7k**, $EC_{50}$ = 0.48 μmol/L) displayed decreased activity.

Taken together, these newly synthesized compounds displayed excellent anti-HIV activities. Since HIV-1 is more prevalent and pathogenic than HIV-2, this study focused on the MOA of the representative compounds in the context of HIV-1.

To determine the target specificity of the new compounds to HIV-1 CA, we, therefore, employed **7b**, **7m**, and **7n** as the three most potent compounds to study a direct interaction with two distinct CA protein constructs: CA monomer and hexamer, using SPR based approach as previously described [27–29]. To assure the validity of experimental findings, **PF74** was used as an in-line control in this assay.

The resulting sensorgrams and the SPR isotherms were illustrated in Figs. S1 and S2 (Supporting information), respectively. Table 2 shows the corresponding kinetic parameter. The kinetic profile of the compounds **7b**, **7m**, **7n**-CA monomer interaction was comparable to that of the lead compound **PF74** with fast association and dissociation rates, and similar equilibrium dissociation constants as compared to **PF74** (Fig. S1 in Supporting information and Table 2). SPR analysis exhibited that the three new compounds robustly interacted with the immobilized disulfide-stabilized CA hexamer and with a kinetic signature that was broadly similar to that of **PF74**. The on-rates of all four compounds were extremely fast, but the off-rates were slightly variable (Fig. S1), with **PF74** having the slowest off-rate (Table 2). Alterations in off-rates for the hexameric CA, correlate with increased binding affinity (Table 2). Despite their varying off-rates, all compounds exhibited affinities with CA hexamer in the μmol/L range from 5- to 11-fold of **PF74**, with **7n** having a marginally upgraded $K_D$ over **7b** and **7m** (0.915, 1.724 and 1.754 μmol/L, respectively). Surprisingly, the interactions of **7b**, **7m** and **7n** with monomer and hexamer followed a similar profile to **PF74**, with a preference for the hexamer. Conclusively, the SPR analysis results demonstrated that these inhibitors retained the target specificity towards HIV-1 capsid.

**Table 2**
SPR results of **7b**, **7m**, **7n**, and **PF74** binding to monomeric and hexameric CA constructs.

| Compd. | $K_D$[a] (μmol/L) | | Ratio[b] | $k_{off}$ ($s^{-1}$) |
|---|---|---|---|---|
| | Monomer | Hexamer | | |
| **7b** | 5.533 ± 0.801 | 1.724 ± 0.216 | 3.209 | 0.225 ± 0.014 |
| **7m** | 6.502 ± 0.609 | 1.754 ± 0.345 | 3.707 | 0.236 ± 0.016 |
| **7n** | 4.351 ± 0.546 | 0.915 ± 0.181 | 4.755 | 0.198 ± 0.014 |
| **PF74** | 3.410 ± 1.310 | 0.159 ± 0.041 | 21.446 | 0.018 ± 0.000 |

[a] All values represent the average response from at least 3 replicates. Error bars represent standard deviation.
[b] Ratio = $K_D^{Monomer}/K_D^{Hexamer}$.

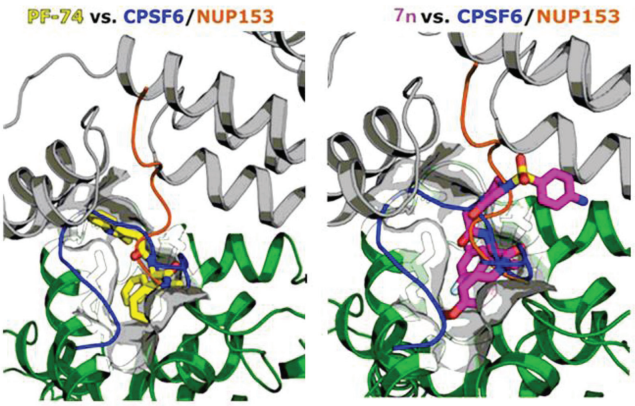


**Fig. 3.** Docking analysis and structural overlay of **PF74** (yellow, PDB code: 4XFZ) and **7n** (purple) compared with CPSF6 (blue) and NUP153 (orange). The co-crystal structures of the CPSF6 (PDB code: 4WYM) peptide and the NUP153 (PDB code: 4U0C) peptide are highlighted in blue and orange, respectively.

To establish whether or not our target compounds genuinely share the same binding pocket as **PF74**, we designed and implemented SPR-based competition assays using peptides generated from the proteins CPSF6 and NUP153, using **7n** as a representative compound. The findings and analysis of these studies were shown in Fig. S3 (Supporting information), which revealed that our immobilized hexameric CA not only has surface activity but also has affinities that are consistent with previously published values [22–30]. Fig. S4 (Supporting information) displays that the competitive ability of **7n** with CPSF6 and NUP153 peptides was comparable to that of **PF74**. Consistent with previously published results [24], **PF74** inhibited the CA hexamer-CPSF6/NUP153 peptides interaction. Remarkably, our newly obtained compound **7n** also inhibited the CA hexamer-CPSF6/NUP153 peptides interaction, suggesting that it was binding within the NTD-CTD interface as expected.

Notably, the inhibition profile of **7n** was opposed to that of **PF74**, with **7n** competing more effectively with NUP153 and **PF74** inhibiting CPSF6 better (Table S1 in Supporting information). To study the possible rationale for this reversal of the inhibitory profile between the two compounds, we used rigorous docking simulations for **PF74** and **7n**, and compared them to the crystal structures of the peptides bound to hexameric CA. Investigation of the docking poses revealed that **7n**, also due to its increased size, occupies a larger space as compared to **PF74** (Fig. 3). The orientation of **7n** was comparable to that of the NUP153 peptide, suggesting

that it might more effectively sterically block the binding site for NUP153.

Using direct engagement of HIV-1 CA monomers/hexamers and competition with CPSF6 and NUP153, we demonstrated low-micromolar affinity binding for **7b** and **7m**, while **7n** engaged hexameric CA in the nanomolar range. The HIV-1 CA protein is essential for the early and late stages of the viral replication cycle. While hexameric/oligomeric CA functions predominantly during the early stages, CA is mainly monomeric during the late stage in the context of newly synthesized Gag polyprotein. We, therefore, sought to determine the stage of inhibition of our most potent compound (**7n**) as a representative for our compound series, using a modified single round infection (SRI) assay, efficiently separating the early and late stages of the HIV-1 life cycle [27].

**PF74** has been shown to have inhibitory characteristics in both the early and late-stages [29]; however, late-stage inhibition was observed only at higher concentrations of **PF74** not used in our setup. As shown in Fig. S5 (Supporting information), **7n** could exert its role in the early and late stages of the HIV-1 life cycle, while **PF74** inhibits only the early stage in our experimental setup. Interestingly, **7n**, although demonstrated as a similar affinity for the monomeric CA protein compared to **PF74**, displayed comparable inhibition in both stages, possibly suggesting a dual mechanism of action.

Besides, we performed MD analysis on **7n**-CA monomer complexes. Fig. S6 (Supporting information) showed the presence of different conformations of the protein and the compound, the whole trajectory was clustered to find the protein and the compound conformations. The clustering procedure produced 19 clusters, the two most populous of which were depicted in Fig. S7 (Supporting information). Site 1 (Fig. S7B) is located at the binding site indicated by the X-ray structure, displays the interactions between the most prominent conformer of **7n** and the HIV-1 CA monomer. Where, Lys70, Met66, Gln63 and Leu56 are shared between the X-ray binding and site 1 of MD simulation binding. The methoxybenzene of **7n** has hydrophobic interactions with Leu56, Met66, and Lys70, and the aminobenzene could have hydrophobic interaction with Lys70. These hydrophobic interactions give the compound tighter binding to this binding site. Also, the aminobenzene could have ion-induced dipole with the ammonium moiety of Lys70, giving further binding affinity for **7n**. Additionally, hydrogen bond analysis showed that **7n** forms hydrogen bonding with Asn57 for 7.0% of the MD simulation time. Fig. S7C shows the binding interactions of **7n** in the second most populated cluster (site 2). During the MD simulation, these two conformations are mainly bound to the NTD region of CA monomer, and there are no critical interactions between the exposed bensulfamide piperazinone structure and this region. Therefore, it can be speculated that the high potency of this series of compounds may be caused by the key interactions between the bensulfamide piperazinone structure and the adjacent monomer.

Since a significant pitfall of **PF74** is its metabolic lability, one of our primary objectives in designing these chemicals was to increase their metabolic half-life. We, therefore, conducted metabolic stability assays of our most potent antiviral compounds (**7b**, **7m**, and **7n**) in both HLM and human plasma, along with **PF74** as a control. **PF74** was rapidly metabolized with a half-life ($t_{1/2}$) of 0.5 min, and improved stability was observed for **7m** ($t_{1/2} = 7.7$ min, 15.4-fold over **PF74**) and **7n** ($t_{1/2} = 2.4$ min, 4.8-fold over **PF74**). The $CL_{int(liver)}$ of **7m** and **7n** was also decreased to 1/16 and 1/5 of that of **PF74**, with values of 161.8, 510.1, and 2576.2 mL/min/kg, respectively (Table S2 in Supporting information). 103.1% of **7b**, 109.2% of **7m**, and 100.4% of **7n** maintained intact after incubation for 120 min at 37 °C. On the contrary, **PF74** was easily metabolized (maintaining amounts of 85.2% at 120 min) (Table S3 in Supporting information). Overall, the representative compounds were comparatively stable in HLM and human plasma, the improvement is most likely due to the introduction of two fluorine atoms on the benzene ring of phenylalanine and the replacement of the indole ring with more minor electron-rich moieties. Due to only modest improvements of the here presented compound series, future efforts will be directed towards further improvement of drug-like properties, including metabolic stability.

In this paper, inspired by the structural and biochemical information of **PF74**, we used a structure-based drug design strategy to design moderators of the capsid NTD-CTD interface that would disrupt HIV-1 replication at multiple stages. This effort generated compound **7n**, which was identified to be the most potent for inhibition of HIV-1 replication and gave a 6.25-fold increment in efficacy to its parent compound **PF74**. Moreover, these inhibitors exhibited a prominent antiviral activity profile against HIV-2 and take compound **7h** as representation whose anti-HIV-2 activity was 139 times that of **PF74**, offering profitable lead compounds as encouraging HIV-2 inhibitor. In this paper, the MOA of representative compounds was discussed only on HIV-1. First, it was shown that **7n** could directly bind to monomeric and hexameric HIV-1 CA with micromolar and nanomolar affinity, respectively. SPR-based competition experiments with CPSF6 and NUP153 peptides have proven that **7n** binds within the NTD-CTD interface of hexameric CA, which is in agreement with our design efforts. SRI experiments displayed that **7n** interferes with the HIV-1 life cycle in a dual-stage manner, influencing both early and late stages. Furthermore, employing MD simulation, we confirmed that **7n** might bind to the same site as **PF74** but with a different direction. Metabolic stability evaluation in HLM and human plasma indicated that **7m** and **7n** has moderately improved stability over **PF74**, providing the rationale for future improvement of the metabolic stability of this compound series.

Taken together, this work culminated in the identification of phenylalanine-bearing HIV-1 capsid inhibitors with a novel chemotype and broad-spectrum anti-HIV activity, and highlights the potential of the NTD-CTD interface in the CA hexameric configuration as a promising target for the design of potent HIV inhibitors.

## Declaration of competing interest

The authors declare that they have no known competing financial interests or personal relationships that could have appeared to influence the work reported in this paper.

## Acknowledgments

We gratefully acknowledge financial support from the National Natural Science Foundation of China (NSFC, Nos. 82173677, 81773574), the Key Project of NSFC for International Cooperation (No. 81420108027), the Shandong Provincial Key Research and Development Project (No. 2019JZZY021011), the Science Foundation for Outstanding Young Scholars of Shandong Province (No. ZR2020JQ31) and NIH/NIAID grant (No. R01AI150491, Cocklin, PI, Salvino, Co-I). We also would like to thank the OpenEye Scientific Software, Inc. for providing a free academic license.

## Supplementary materials

Supplementary material associated with this article can be found, in the online version, at doi:10.1016/j.cclet.2022.06.034.

## References

[1] S. Moir, T.W. Chun, A.S. Fauci, Annu. Rev. Pathol. 6 (2011) 223–248.
[2] K.D. Pedro, L.M. Agosto, J.A. Sewell, et al., Proc. Natl. Acad. Sci. U. S. A. 118 (2021) e2012835118.

[3] UNAIDS, Global HIV & AIDS statistics–2020 fact sheet, United Nations (12 June 2022) https://www.unaids.org/en/resources/fact-sheet. accessed on.
[4] J. Esbjörnsson, M. Jansson, S. Jespersen, et al., AIDS Res. Ther. 16 (2019) 24.
[5] J. Ghosn, B. Taiwo, S. Seedat, et al., Lancet 392 (2018) 685–697.
[6] A.B. Kleinpeter, E.O. Freed, Viruses 12 (2020) 940.
[7] P. Zhan, C. Pannecouque, E. De Clercq, et al., J. Med. Chem. 59 (2016) 2849–2878.
[8] Y. Ma, E. Frutos-Beltrán, D. Kang, et al., Chem. Soc. Rev. 50 (2021) 4514–4540.
[9] J. Du, J. Guo, D. Kang, et al., Chin. Chem. Lett. 31 (2020) 1695–1708.
[10] C. Mendoza, A.B. Lozano, E. Caballero, et al., AIDS Rev. 22 (2020) 44–56.
[11] L. Sun, X. Zhang, S. Xu, et al., Eur. J. Med. Chem. 217 (2021) 113380.
[12] S. Xu, L. Sun, B. Huang, et al., Future Med. Chem. 12 (2020) 1281–1284.
[13] E.M. Campbell, T.J. Hope, Nat. Rev. Microbiol. 13 (2015) 471–483.
[14] A. Dharan, E.M. Campbell, Curr. Opin. Virol. 53 (2022) 101203.
[15] L. Wang, M.C. Casey, S.K.V. Vernekar, et al., Acta. Pharm. Sin. B 11 (2021) 810–822.
[16] W.M. McFadden, A.A. Snyder, K.A. Kirby, et al., Retrovirology 18 (2021) 41.
[17] S. Zhuang, B.E. Torbett, Viruses 13 (2021) 417.
[18] A. Guedán, C.D. Donaldson, E.R. Caroe, et al., PLoS Pathog. 17 (2021) e1009484.
[19] D.A. Bejarano, K. Peng, V. Laketa, et al., eLife 8 (2019) e41800.
[20] A. Guedán, E.R. Caroe, G.C.R. Barr, et al., Viruses 13 (2021) 1425.
[21] K.A. Matreyek, S.S. Yücel, X. Li, et al., PLoS Pathog. 9 (2013) e1003693.
[22] A. Bhattacharya, S.L. Alam, T. Fricke, et al., Proc. Natl. Acad. Sci. U. S. A. 111 (2014) 18625–18630.
[23] J. Shi, J. Zhou, U.D. Halambage, et al., J. Virol. 89 (2015) 208–219.
[24] A.J. Price, D.A. Jacques, W.A. McEwan, et al., PLoS Pathog. 10 (2014) e1004459.
[25] S. Rankovic, R. Ramalho, C. Aiken, et al., J. Virol. 92 (2018) e00845-18.
[26] W. Wei, S. Cherukupalli, L. Jing, et al., Drug Discov. Today 25 (2020) 1839–1845.
[27] J.P. Xu, A.C. Francis, M.E. Meuser, et al., J. Drug Des. Res. 5 (2018) 1070.
[28] M.E. Meuser, P.A.N. Reddy, A. Dick, et al., J. Med. Chem. 64 (2021) 3747–3766.
[29] S. Xu, L. Sun, A. Dick, et al., Eur. J. Med. Chem. 227 (2022) 113903.
[30] X. Zhang, L. Sun, M.E. Meuser, et al., Eur. J. Med. Chem. 226 (2021) 113848.